Hydrodynamic interactions enhance gelation in dispersions of colloids with short-ranged attraction and long-ranged repulsion

Zsigmond Varga and James Swan*
Department of Chemical Engineering, MIT, Cambridge MA 02139, USA
*Corresponding author: jswan@mit.edu

Supplementary Information

We present results on msd, local bond order parameters and $F_S(q,t)$ and $F(q,t)$ measurements for the experimental conditions analyzed by Campbell and coworkers[16]: $\phi = 0.11$, $U_A(2a) = -13kT$, $\delta = 0.13$, $A = 8k_BT$ and $\kappa a = 0.8$.

Microstructure and local order

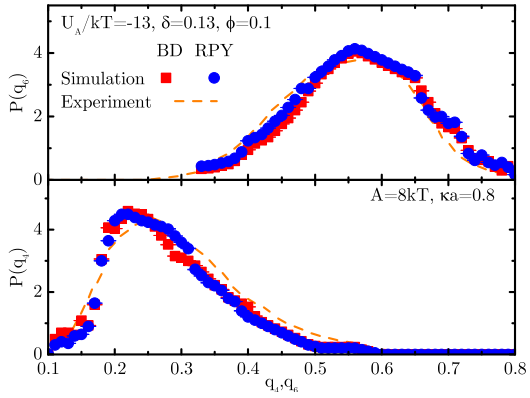

Figure 1 q_4 and q_6 bond-order distributions in BD and RPY simulations for the experimental conditions $\phi = 0.11$, $U_A(2a) = -13kT$, $\delta = 0.13$, $A = 8kT$ and $\kappa a = 0.8$ at $t = 10^3\tau_D$. Error bars represent sample to sample fluctuations over ten independently generated instances. Also shown are experimental results.

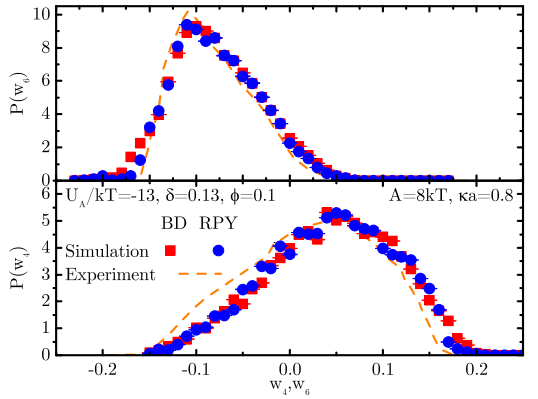

Figure 2 $\hat{w}_4$ and $\hat{w}_6$ bond-order distributions in BD and RPY simulations for the experimental conditions $\phi = 0.11$, $U_A(2a) = -13kT$, $\delta = 0.13$, $A = 8kT$ and $\kappa a = 0.8$ at $t = 10^3\tau_D$. Error bars represent sample to sample fluctuations over ten independently generated instances. Also shown are experimental results.

Campbell and coworkers provide measurements of the local bond order parameters at one specified condition. We The distributions for the gels generated in simulations with BD and RPY compare very well with the experiment, especially with respect to the degree of tetrahedral symmetry observed and capturing the broad distribution of the q_4 and q_6 parameters. work

strands is essentially the same in both simulation methods. As before, we find that once percolation has occurred, the local microstructural environment around the particles is very close to the thermodynamically predicted tetrahedral symmetry of Bernal spirals and the kinetics dictated by hydrodynamic flows are negligible. However, as the scattering results show, even at these conditions there remain differences between the two hydrodynamic models in terms of the relaxation dynamics of the network.

Mean squared displacement

For the highest attraction strength we observe dynamic arrest for both BD and RPY. At short times, the MSD is again larger for the RPY simulations, which correctly account for long-ranged hydrodynamic interactions. We observe a pronounced plateau in both RPY and BD that suggest very similar localization lengths. For high quenches of $-13kT$ compaction rates are greatly reduced relative to coagualtion so that percolation is mainly driven by the thermodynamics and hydrodynamic interactions have a minor role.

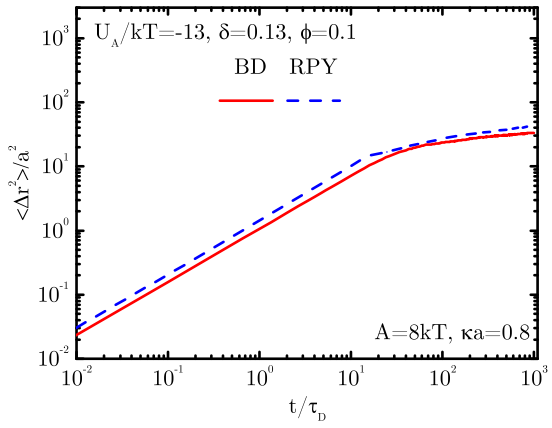

Figure 3 Mean squared displacement in BD and RPY simulations for the for the experimental conditions $\phi = 0.11$, $U_A(2a) = -13kT$, $\delta = 0.13$, $A = 8kT$ and $\kappa a = 0.8$ after a waiting time of $t_w = 10\tau_D$.

Gelation dynamics

As expected, both with and without long-ranged hydrodynamics, single-particle and collective motion is noticeably suppressed and exhibit signs of percolation (see figures 4 and 5). As already seen for dispersions at $U_A(2a) = -10kT$, for large quenches beyond the percolation boundary, single particle motion is dictated by the thermodynamics not long-ranged hydrodynamics and the two different kinetic models produce only small disagreements (see also β_S). In contrast we observe statistically significant differences in $F(q,t)$ and significantly faster relaxation times for RPY (see insets) attributable to the role of long-ranged hydrodynamic interactions in the collective motion of the gel. Differences in the relaxation dynamics persist for deep quenches and ultimately will affect the mechanical response of the material. Network restructuring and a broad relaxation spectrum are observed in both BD and RPY (see β_I), however the modes are till quite different depending on the hydrodynamic model.

Movies

We visually illustrate the different relaxation dynamics between BD and RPY gels at the same conditions. Movies 1 and 2 show the 100 bare diffusion steps at conditions: $\phi = 0.15$, $U_A(2a) = -10kT$, $\delta = 0.1$, $\kappa a = 0.8$ and $A = 8kT$ for BD and RPY respectively.

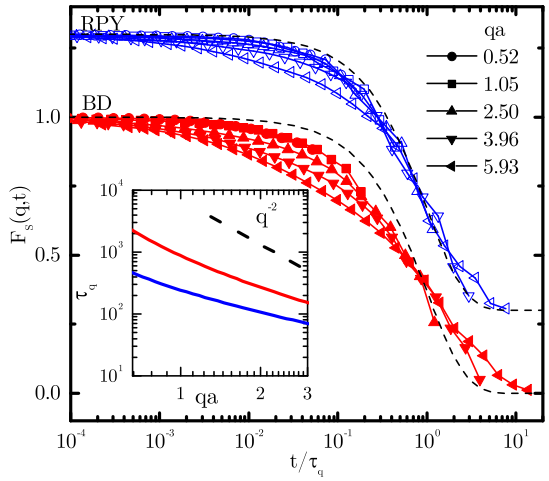

Figure 4 The incoherent scattering function $F_s(q,t)$ for BD and RPY gels with $\phi = 0.11$, $\delta = 0.13$, $A = 8kT$, $\kappa a = 0.8$ and $U_A(2a) = -13kT$ for selected wave vectors q at $t = 500\tau_D$. For clarity, a constant vertical offset of 0.3 units was added between sets of $F_s(q,t)$. The dashed lines present the trivial exponential $\exp\left(-t/\tau_q\right)$ to emphasize the compressed and stretched nature of the scattering function decay. Sample to sample fluctuations over five independently generated instances correspond to deviations of $\pm 3\%$ - error bars not shown. Inset: the characteristic relaxation time τ_q as a function of q for the two different dispersions - colors are the same as in the main plot.

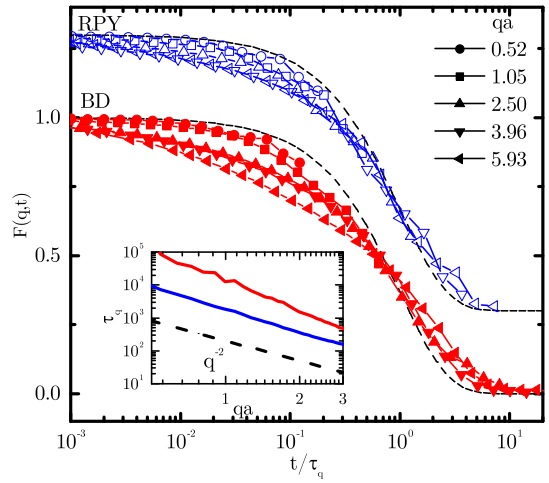

Figure 5 The coherent scattering function $F(q,t)$ for BD and RPY gels with $\phi = 0.11$, $\delta = 0.13$, $A = 8kT$, $\kappa a = 0.8$ and $U_A(2a) = -13kT$ for selected wave vectors q at $t = 500\tau_D$. For clarity, a constant vertical offset of 0.3 units was added between sets of $F(q,t)$. The dashed lines present the trivial exponential $\exp\left(-t/\tau_q\right)$ to emphasize the compressed and stretched nature of the scattering function decay. Sample to sample fluctuations over five independently generated instances correspond to deviations of $\pm 2\%$ - error bars not shown. Inset: the characteristic relaxation time τ_q as a function of q for the two dispersions - colors are the same as in the main plot.

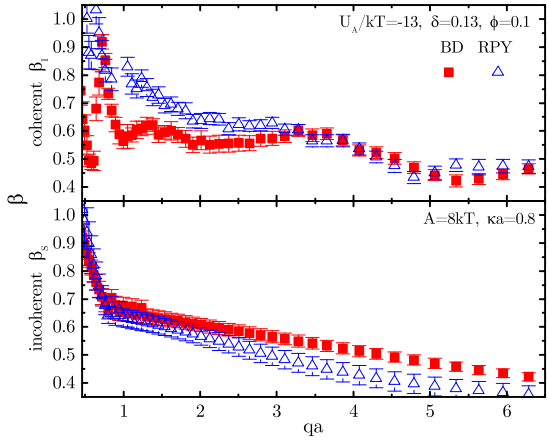

Figure 6 Stretching exponent β of $F(q,t)$ (coherent, top) and $F_S(q,t)$ (incoherent, bottom) of BD and RPY gels with $\phi = 0.11$, $\delta = 0.13$, $A = 8kT$, $\kappa a = 0.8$ and $U_A(2a) = -13kT$ for selected wave vectors q at $t = 500\tau_D$. Sample to sample fluctuations were measured over five independently generated instances.